Modeling and Compensation of Nonlinearities and Friction in a Micro Hard Disk Drive Servo System With Nonlinear Feedback Control

Kemao Peng, Ben M. Chen, *Senior Member, IEEE*, Guoyang Cheng, *Student Member, IEEE*, and Tong H. Lee

Abstract—Friction and nonlinearities result in large residual errors and deteriorate the performance of head positioning of hard disk drive (HDD) servo systems and other mechanical servo systems. Thus, it is highly desirable to characterize the behaviors of nonlinearities and friction in the servo systems. This paper presents a fairly comprehensive modeling and compensation of friction and nonlinearities of a typical voice-coil-motor (VCM) actuator used in commercial HDDs, and the design of an HDD servo system using an enhanced nonlinear control technique. Our contributions are two-fold: We will first obtain a complete model of the VCM actuator including friction and nonlinear characteristics through a careful examination of the configuration and structure of the actual system and through a thorough analysis of its physical effects together with its time-domain and frequency-domain responses. We will then proceed to design a servo system for the hard drive using an enhanced composite nonlinear feedback (CNF) control technique with a simple friction and nonlinearity compensation scheme. The enhanced CNF technique has a feature of removing the uncompensated portion of friction and nonlinearities without sacrificing the overall tracking performance. Simulation and experimental results for both the modeling and the servo design show that our approach is very effective and successful. In particular, our experimental results show that the enhanced CNF control has outperformed the conventional proportional-integral-derivative (PID) control in settling time by 76%. We believe that this approach can be adopted to solve other servomechanism problems.

Index Terms—Actuators, friction, hard disks, identification, modeling, motion control, nonlinearities, servo systems.

I. INTRODUCTION

PRESENTLY, most hard disk drive (HDD) servo systems use a voice-coil-motor (VCM) actuator to actuate the read/write (R/W) recording arm assembly, which consists of a pivot with a ball bearing, a metal arm, and a rigid suspension that holds the R/W head and slider (see Fig. 1). The VCM is a typical dc motor that translates an input current to a force or acceleration as its output. Its frequency domain response without considering friction and nonlinearities matches very well to that of a double integrator [7] at low-frequency range, typically from dc to somewhere around 1–2 kHz, and has many high-frequency resonance modes. Unfortunately, it can be observed that nonlinearities from friction in the actuator rotary pivot bearing and data flex cable in the VCM actuator generate large residual errors and deteriorate the performance of head positioning of HDD servo systems, which is much more severe in the track following stage when the R/W head is moving from the current track to its neighborhood tracks. The desire to fully understand the behaviors of nonlinearities and friction in the servo systems is obvious. Actually, this motivates us to carry out a complete study and modeling of the friction and nonlinearities for the VCM actuated HDD servo systems.

Friction is hard nonlinear and may result in residual errors, limit cycles and poor performance [3]–[5], [24]. Friction exists in almost all servomechanisms, behaves in features of Stribeck effect, hysteresis, stiction and varying break-away force, occurs in all mechanical systems and appears at the physical interface between two surfaces moving in contact with each other. The features of friction have been extensively studied [3]–[5], [10], [16], [22], [24], but there is significant difference among diverse systems. There has been a significantly increased interest in friction in the industries, which is driven by strong engineering needs in a wide range of industries and availability of both precise measurement and advanced control techniques.

The HDD industry persists in need for companies to come up with devices that are cheaper and able to store more data and retrieve or write to them at faster speed. Decreasing the HDD track width is a feasible idea to achieve these objectives. But, the presence of friction in the rotary actuator pivot bearing results in large residual errors and high-frequency oscillations, which may produce larger positioning error signal to hold back the further decreasing of the track width and to deteriorate the performance of the servo systems. This issue becomes more noticeable for small drives and is one of the challenges to design head positioning servo systems for small HDDs. Much effort has been put into the research on mitigation of the friction in the pivot bearing in the HDD industry in the last decade [1], [18], [19], [27], [28]. It is still ongoing in the disk-drive industry [6], [17], [21].

Diverse modeling methods had been proposed [14], [17] based on linear systems, where nonlinearities of plants are assumed to be tiny and can be neglected. As such, these methods cannot be directly applied to model plants with nonlinearities. A method had been proposed in [3] to estimate the parameters of friction for typical dc motors, but it is inappropriate for the VCM actuator because of insufficient information available in HDD servo systems, in which only the relative displacement of the R/W head is measurable. One of the key

Fig. 1. Typical HDD with a VCM actuator.

Fig. 2. Mechanical structure of a typical VCM actuator.
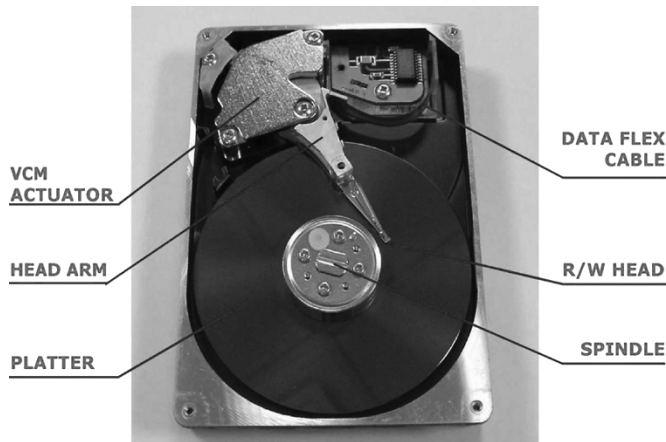
issues to model systems with nonlinearities is to determine the physical structures of the nonlinear components. Another issue is that there is generally no analytical solution for nonlinear differential equations, which causes trouble in identifying the model parameters. In the first part of this paper, we utilize the physical effect approach of [11] to determine the structures of nonlinearities and friction associated with the VCM actuator in a typical HDD servo system. This will be done by carefully examining and analyzing physical effects that occur in or between electromechanical parts. Then, we will employ a Monte Carlo process [12], [13], [23] to identify the parameters in the structured model. We note that Monte Carlo methods are very effective in approximating solutions to a variety of mathematical problems, for which their analytical solutions are hard, if not impossible, to be determined. Our simulation and experimental results show that the identified model of friction and nonlinearities using such approaches matches very well the behavior of the actual system.

The second part of this paper focuses on the controller design for the HDD servo system. Our philosophy of designing servo systems is rather simple. Once the model of the friction and nonlinearities of the VCM actuator is obtained, we will try to cancel as much as possible all these unwanted elements in the servo system. As it is impossible to have perfect models for friction and nonlinearities, a perfect cancellation of these elements is unlikely to happen in the real world. We will then formulate our design by treating the uncompensated portion as external disturbances. An enhanced composite nonlinear feedback (CNF) control technique, which is an extension of our early works [7], [8], will thus be proposed and used to carry out our servo system design. Compared to the result of [7] and [8], the new technique has an additional feature of removing constant bias and rejecting disturbances. Simulation and implementation results show that our approach is very efficient and successful.

The outline of this paper is as follows. In Section II, a structural model of friction and nonlinearities in the VCM actuator will be determined through the physical effect analysis, and its parameters will be identified using the Monte Carlo method and verified. Section III presents the theory of the enhanced CNF control technique. An HDD servo system design with friction
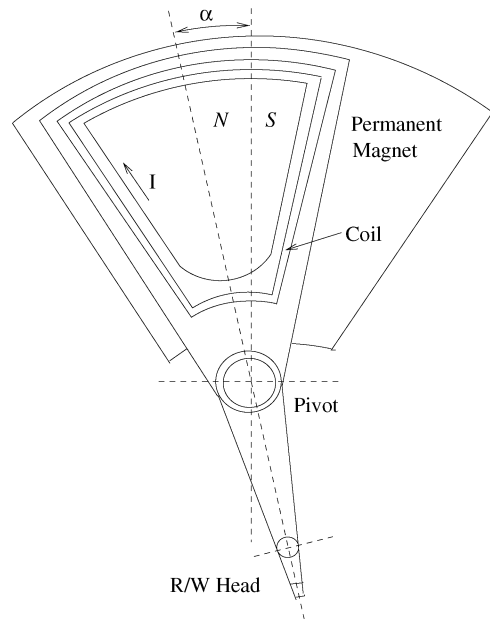
and nonlinearities compensation using the enhanced CNF technique will then be carried out in Section IV. Finally, we draw some concluding remarks in Section V.

II. MODELING OF THE VCM ACTUATOR

The mechanical structure of a typical VCM actuator is shown in Fig. 2. The motion of the coil is driven by a permanent magnet similar to typical dc motors. The stator of the VCM is built of a permanent magnet. The rotor consists of a coil, a pivot, and a metal arm on which the R/W head is attached. A data flex cable is connected with the R/W head through the metal arm to transfer data read from or written to the HDD disk via the R/W head. Typically, the rotor has a deflected angle, α in rad, ranging up to 0.5 rad in commercial disk drives. We are particularly interested in the modeling of the friction and nonlinearities for the actuator in the track following stage, in which the R/W head movement is within the neighborhood of its current track and, thus, $\alpha \ll 1$. An IBM microdrive (DMDM-10 340) is used throughout for illustration.

A. Structural Model of the VCM Actuator

We first adopt the physical effect analysis of [11] to determine the structures of nonlinearities in the VCM actuator. It is to analyze the effects between the components of the actuator, such as the stator, rotor and support plane as well as the VCM driver. The actuator is designed to position the R/W head fast and precisely onto the target track, and is driven by a driver, a full bridge power amplifier, which converts an input voltage into an electric current. The electric circuit of a typical VCM driver is shown in Fig. 3, where Z represents the coil of the actuator and the external input voltage is exerted directly into the driver to drive the coil.

In order to simplify our analysis, we assume that the physical system has the following properties: 1) the permanent magnet
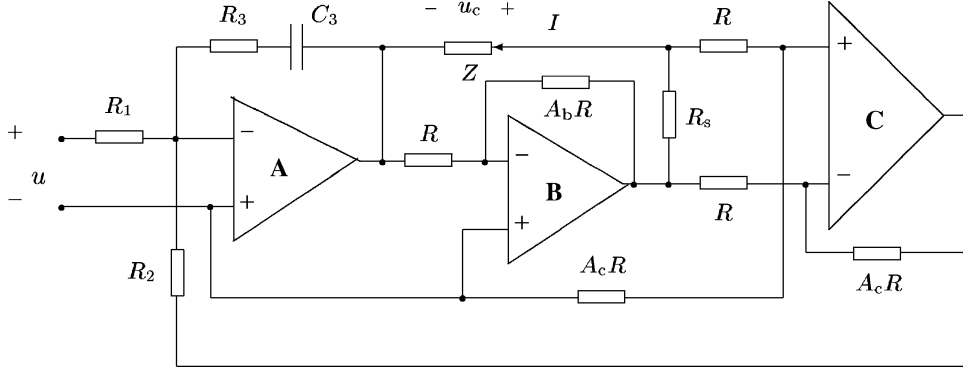
Fig. 3.   Electric circuit of a typical VCM driver.

is constant; and 2) the coil is assembled strictly along the radius and concentric circle of the pivot. Furthermore, we assume that the friction of a mechanical object consists of Coloumb friction and viscous damping, and is characterized by a typical friction function as the following:

$$
\begin{aligned}
&f(F_{\mathrm{N}}, F_{\mathrm{e}}, v, \mu_{\mathrm{d}}, \mu_{\mathrm{s}}, \mu_{\mathrm{v}}) \\
&= \begin{cases}
-\mu_{\mathrm{d}} F_{\mathrm{N}} \mathrm{sgn}(v) - \mu_{\mathrm{v}} v, & v \neq 0 \\
-F_{\mathrm{e}}, & v = 0, |F_{\mathrm{e}}| \leq \mu_{\mathrm{s}} F_{\mathrm{N}} \\
-\mu_{\mathrm{s}} F_{\mathrm{N}} \mathrm{sgn}(F_{\mathrm{e}}), & v = 0, |F_{\mathrm{e}}| > \mu_{\mathrm{s}} F_{\mathrm{N}}
\end{cases}
\end{aligned} \tag{1}
$$

where f is the friction force, F_{N} is the normal force, i.e., the force perpendicular to the contacted surfaces of the objects, F_{e} is the external force applied to the object, v is the relative moving speed between two contact surfaces, and $\mu_{\mathrm{s}} F_{\mathrm{N}}$ is the break-away force. Furthermore, $\mu_{\mathrm{d}}, \mu_{\mathrm{s}}$, and μ_{v} are, respectively, the dynamic, static and viscous coefficients of friction.

Through a detailed analysis of the VCM driver circuit in Fig. 3, it is straightforward to verify that the relationship between the driver input voltage and the current and voltage of the VCM coil is given by

$$
\begin{aligned}
&\frac{R_{\mathrm{s}} + (1 + A_{\mathrm{c}})(1 + A_{\mathrm{b}})R}{R_{\mathrm{s}} A_{\mathrm{c}}(1 + A_{\mathrm{c}})(1 + A_{\mathrm{b}})R} \cdot \frac{R_2}{R_1} u \\
&\qquad = \frac{1 + s\left[R_3 + \frac{R_2}{A_{\mathrm{c}}(1+A_{\mathrm{b}})}\right] C_3}{1 + s R_3 C_3} I + \mathcal{E}(s) u_{\mathrm{c}}
\end{aligned} \tag{2}
$$

where

$$
\begin{aligned}
\mathcal{E}(s) &= \frac{A_{\mathrm{b}}}{(1 + A_{\mathrm{c}})(1 + A_{\mathrm{b}})R} \\
&\quad \times \frac{1 + s\left[R_3 + \frac{R_2}{A_{\mathrm{c}} A_{\mathrm{b}}}\left(1 + \frac{R(1+A_{\mathrm{c}})}{R_{\mathrm{s}}}\right)\right] C_3}{1 + s R_3 C_3}
\end{aligned} \tag{3}
$$

u is the input voltage to the driver, I and u_{c} are, respectively, the VCM coil current and voltage. For the IBM microdrive (DMDM-10 340) used in our tests, $R_1 = 8.2 \mathrm{~K\Omega}$, $R_2 = 1 \mathrm{~K\Omega}$, $R_3 = 270 \mathrm{~K\Omega}$, $R_{\mathrm{s}} = 1 \mathrm{~\Omega}$, $R = 16 \mathrm{~K\Omega}$, $C_3 = 270 \mathrm{~pF}$, and the amplifier gains $A_{\mathrm{c}} = 2$ and $A_{\mathrm{b}} = 4.7$. For such a drive, we have

$$
\mathcal{E}(s) = \frac{1.7178 \times 10^{-5}(1 + 1.45 \times 10^{-3} s)}{1 + 7.29 \times 10^{-5} s} \tag{4}
$$

which has a magnitude response ranging from -95 dB (for frequency less than 110 Hz) to -69 dB (for frequency greater than 2.2 kHz), and

$$
\frac{1 + s\left[R_3 + \frac{R_2}{A_{\mathrm{c}}(1+A_{\mathrm{b}})}\right] C_3}{1 + s R_3 C_3} \approx 1, \quad \text{for all } s. \tag{5}
$$

Such a property generally holds for all commercial disk drives. As such, it is safe to approximate the relationship of u and I of the VCM driver as

$$
I = \frac{R_2}{A_{\mathrm{c}} R_1 R_{\mathrm{s}}} u = k_{\mathrm{vd}} u. \tag{6}
$$

For the IBM microdrive used in our experiment throughout this work, $k_{\mathrm{vd}} = 0.061 \mathrm{~\Omega}^{-1}$.

Next, it is straightforward to derive that the torque T_{m}, relative to center of the pivot and that along anti-clockwise is positive and produced by the permanent magnet B_{coil} in the coil with the electric current, is given by

$$
T_{\mathrm{m}} = \left(r_1^2 - r_2^2\right) B_{\mathrm{coil}} n_{\mathrm{coil}} k_{\mathrm{vd}} u \tag{7}
$$

r_1 and r_2 are, respectively, the outside and inside radius of the coil to center of the pivot, and n_{coil} is number of windings of the coil. The total external torque T_{e} applied to the VCM actuator is given as follows:

$$
T_{\mathrm{e}} = T_{\mathrm{m}} - T_{\mathrm{c}}(\alpha) \tag{8}
$$

where $T_{\mathrm{c}}(\alpha)$ is the spring torque produced by the data flex cable and is a function of the deflection angle α or the displacement of the R/W head. The friction torque presented in the VCM actuator comes from two major sources. One is the friction in the pivot bearing and the other is between the pivot bearing and the support plane. The friction torque in the pivot bearing can be characterized as

$$
T_{\mathrm{f1}} = f(F_{\mathrm{N1}}, F_{\mathrm{e1}}, r_3 \dot{\alpha}, \mu_{\mathrm{d1}}, \mu_{\mathrm{s1}}, \mu_{\mathrm{v1}}) r_3 \tag{9}
$$

where F_{e1} is the external force, $\mu_{\mathrm{d1}}, \mu_{\mathrm{s1}}$, and μ_{v1} are the related friction coefficients as defined in (1), r_3 is the radius of the pivot to its center, and

$$
F_{\mathrm{N1}} = \left|F_{\mathrm{r}} + m_{\mathrm{r}}(\dot{\alpha})^2\right| \tag{10}
$$

is the normal force, which consists of the centrifugal force of the rotor and the diametrical force, F_r. Furthermore, m_r is a constant dependent on the mass distribution of the rotor, and

$$F_r = 2(r_1 - r_2)B_{coil}n_{coil}k_{vd}u\alpha \qquad (11)$$

is the force along the radius of the pivot bearing produced in the coil by the permanent magnet. The friction torque between the pivot bearing and the support plane can be characterized as

$$T_{f2} = f(F_{N2}, F_{e2}, r_3\dot{\alpha}, \mu_{d2}, \mu_{s2}, \mu_{v2})r_3 \qquad (12)$$

where F_{e2} is the external force, μ_{d2}, μ_{s2}, and μ_{v2} are the related friction coefficients as defined in (1), and

$$F_{N2} = |T_0|r_3^{-1} \qquad (13)$$

is the normal force resulted from a static balance torque of the rotor, T_0. Thus, the total friction torque T_f presented in the VCM actuator is given by

$$T_f = T_{f1} + T_{f2} = \begin{cases} -T_v, & \dot{\alpha} \neq 0 \\ -T_e, & \dot{\alpha} = 0, |T_e| \leq T_s \\ -T_s \mathrm{sgn}(T_e), & \dot{\alpha} = 0, |T_e| > T_s \end{cases} \qquad (14)$$

where

$$T_v = \left[\mu_{d1}\left|2(r_1 - r_2)B_{coil}n_{coil}k_{vd}u\alpha + m_r(\dot{\alpha})^2\right|r_3 + \mu_{d2}|T_0|\right] \\ \times \mathrm{sgn}(\dot{\alpha}) + (\mu_{v1} + \mu_{v2})r_3^2\dot{\alpha} \qquad (15)$$

and

$$T_s = 2\mu_{s1}\left|(r_1 - r_2)B_{coil}n_{coil}k_{vd}u_0\alpha_0\right|r_3 + \mu_{s2}|T_0| \qquad (16)$$

is the break-away torque, and where u_0 and α_0 are, respectively, the corresponding input voltage and the deflection angle for the situation when $\dot{\alpha} = 0$.

Lastly, it is simple to verify that the relative displacement of the R/W head, y, is given by

$$y = 2r_4 \sin\frac{\alpha}{2} \approx r_4\alpha, \quad |\alpha| \ll 1 \qquad (17)$$

where r_4 is the length from the R/W head to the center of the pivot. Following the Newton's law of motion $J\ddot{\alpha} = T_e + T_f$ where J is the moment of the inertia of the VCM rotor, we have:

$$\ddot{y} = -\tilde{T}_c + \tilde{T}_f + bu \qquad (18)$$

where

$$\tilde{T}_f = \begin{cases} -\left[\left|d_1buy + d_2(\dot{y})^2\right| + d_3\right] \\ \quad \times \mathrm{sgn}(\dot{y}) - d_0\dot{y}, & \dot{y} \neq 0, \\ -\tilde{T}_e, & \dot{y} = 0, |\tilde{T}_e| \leq \tilde{T}_s \\ -\tilde{T}_s \mathrm{sgn}(\tilde{T}_e), & \dot{y} = 0, |\tilde{T}_e| > \tilde{T}_s \end{cases} \qquad (19)$$

and

$$\left.\begin{array}{l} \tilde{T}_e = -\tilde{T}_c(y) + bu, \\ \tilde{T}_s = d_4b|u_0y_0| + d_5 \\ \tilde{T}_c = J^{-1}r_4T_c(\alpha) \\ b = J^{-1}r_4\left(r_1^2 - r_2^2\right)B_{coil}n_{coil}k_{vd} \\ d_0 = J^{-1}(\mu_{v1} + \mu_{v2})r_3^3 \\ d_1 = 2r_3\mu_{d1}\left[r_4(r_1 + r_2)\right]^{-1} \\ d_2 = r_3m_r\mu_{d1}(Jr_4)^{-1} \\ d_3 = J^{-1}r_4\mu_{d2}|T_0| \\ d_4 = 2r_3\mu_{s1}\left[r_4(r_1 + r_2)\right]^{-1} \\ d_5 = J^{-1}r_4\mu_{s2}|T_0| \end{array}\right\} \qquad (20)$$

with u_0 and y_0 being, respectively, the corresponding input voltage and the displacement for the case when $\dot{y} = 0$.

It is clear now that the expressions in (18)–(20) give a complete structure of the VCM model including friction and nonlinearities from the data flex cable. Our next task is to identify all these parameters for the IBM microdrive (DMDM-10 340).

B. Identification and Verification of Model Parameters

We proceed to identify the parameters of the VCM actuator model given in (18)–(20). We note that there are results available in [3] to estimate friction parameters for typical dc motors for which both velocity and displacement are measurable and without constraint. Unfortunately, for the VCM actuator studied in this paper, it is impossible to measure the time-domain in constant velocity motions and only the relative displacement of the R/W head is measurable. As such, the method of [3] cannot be adopted to solve our problems. Instead, we will employ the popular Monte Carlo method [12], [13], [23], which has been widely used in solving engineering problems and is capable of providing good numerical solutions.

First, it is simple to obtain from (18) at a steady state when $\dot{y} = 0$ and $\ddot{y} = 0$

$$\begin{aligned} \left|u_0 - b^{-1}\tilde{T}_c(y_0)\right| &= b^{-1}|\tilde{T}_f| \\ &\leq b^{-1}\tilde{T}_s \\ &= d_4|u_0y_0| + b^{-1}d_5. \end{aligned} \qquad (21)$$

Our experimental results show that the right-hand side of (21) is very insignificant for small input signal u_0 and small displacement y_0. This will be verified later when the model parameters are fully identified. Thus, we have

$$u_0 \approx b^{-1}\tilde{T}_c(y_0) := \tilde{T}_{bc}(y_0) \qquad (22)$$

which will be used to identify $\tilde{T}_c(y)$ or equivalently $T_c(\alpha)$, the spring torque produced by the data flex cable. Next, for the small neighborhood of (u_0, y_0), we can rewrite the dynamic equation of (18) as

$$\ddot{y} = -\left.\frac{\partial\tilde{T}_c}{\partial y}\right|_{y=y_0}(y - y_0) + b(u - u_0) + \tilde{T}_f. \qquad (23)$$

For small signals and by omitting the nonlinear terms in $\tilde{T}_{\mathrm{f}}$, the dynamic equation (23) can be approximated by a second-order linear system with a transfer function from $u - u_0$ to $y - y_0$

$$G_{y_0, u_0}(s) = \frac{b}{s^2 + d_0 s + \omega_{\mathrm{p}}^2}. \tag{24}$$

The natural frequency of the previous transfer function (or roughly its peak frequency), ω_{p}, is given by

$$\omega_{\mathrm{p}} = \left(\left. \frac{\partial \tilde{T}_{\mathrm{c}}}{\partial y} \right|_{y = y_0} \right)^{\frac{1}{2}} \tag{25}$$

and its static gain is given by $k_{\mathrm{dc}} = b\omega_{\mathrm{p}}^{-2}$, which implies that

$$b = k_{\mathrm{dc}}\omega_{\mathrm{p}}^2 = 4\pi^2 k_{\mathrm{dc}} f_{\mathrm{p}}^2 \tag{26}$$

where $f_{\mathrm{p}} = \omega_{\mathrm{p}}/(2\pi)$. Expression in (26) will be used to estimate the parameter b. More specifically, the parameters of the dynamic models of the VCM actuator will be identified using the following procedure.

1) The nonlinear characteristics of the data flex cable or equivalently $\tilde{T}_{\mathrm{bc}}(y)$ will be initially determined using (22) with a set of input signal, u_0, and its corresponding output displacement, y_0. It will be fine tuned later using the Monte Carlo method.
2) The parameter b will be initially calculated using the measured static gains and peak frequencies as in (26), resulting from the dynamical responses of the actuator to a set of small input signals. Again, the identified parameter will be fine tuned later using the Monte Carlo method.
3) All system parameters will then be identified using the Monte Carlo method to match the frequency response to small input signal.
4) The high-frequency resonance modes of the actuator, which have not been included in either (18) or (23), will be determined from frequency responses to input signals at high frequencies.

The previous procedure will yield a fairly complete and comprehensive model including nominal dynamics, high-frequency resonance modes, friction and nonlinearities of the VCM actuator. In our experiments, the relative displacement of the R/W head is the only measurable output and is measured using a laser doppler vibrometer (LDV). A dynamic signal analyzer (DSA) (Model SRS 785) is used to measure the frequency responses of the VCM actuator. The DSA is also used to record both input and output signals of time-domain responses. Square waves are generated with a dSpace DSP board installed in a personal computer.

The time-domain response of the VCM actuator to a typical square input signal about 1 Hz is shown as Fig. 4. With a group of time-domain responses to a set of square input signals, we obtain the corresponding measurement data for the nonlinear function $\tilde{T}_{\mathrm{bc}}(y_0)$ which can be matched pretty nicely by an arctan function (see Fig. 5) as the following:

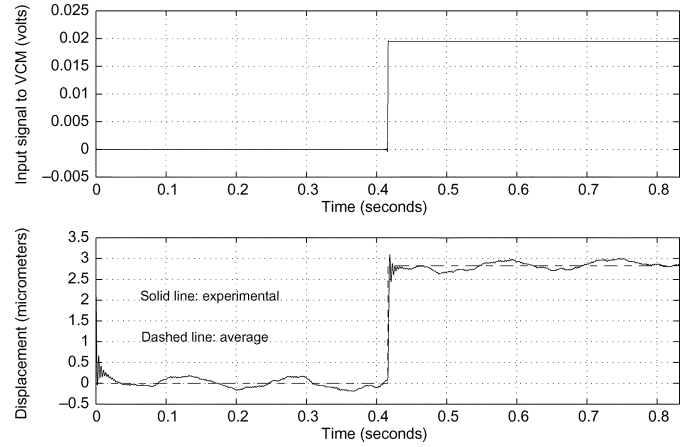$$\tilde{T}_{\mathrm{bc}}(y) = a \arctan(cy) \tag{27}$$

Fig. 4.   Time-domain response of the VCM actuator to a square wave input.
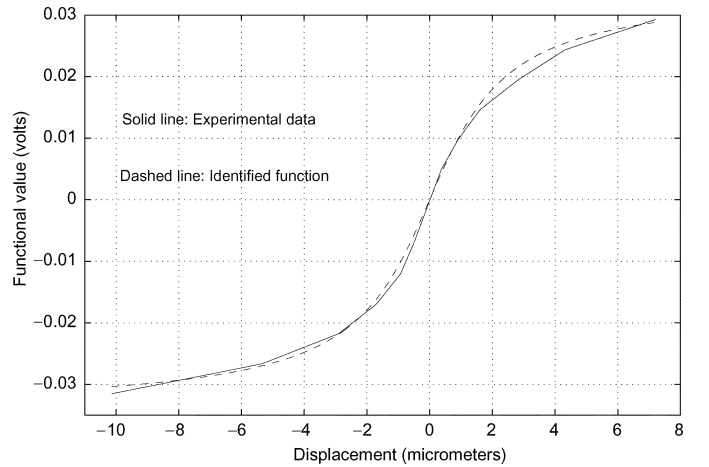

Fig. 5.   Nonlinear characteristics of the data flex cable.

where $a = 21.8748 \times 10^{-3}$ V and $c = 0.5351 (\mu\mathrm{m})^{-1}$. These parameters will be further fine tuned later in the Monte Carlo process.

Next, by fixing a particular input offset point u_0 and by injecting on top of u_0 a sweep of small sinusoidal signals with an amplitude of 1 mV, we are able to obtain a corresponding frequency response within the range of interest. It then follows from (26) that the values of the static gain k_{dc} and peak frequency f_{P} of the frequency response can be used to estimate the parameter, b. Fig. 6 shows the frequency response of the system for the pair $(u_0, y_0) = (0, 0)$, which gives a static gain of 63.71 and a peak frequency of 305.24 Hz. In order to obtain a more accurate result, we repeat the previous experimental tests for several pairs (u_0, y_0) and the results are shown in Table I. The parameter b can then be more accurately determined from these data using a least square fitting

$$\min_{b} \sum_{i=1}^{7} \left[b - k_{\mathrm{dc}, i} \omega_{\mathrm{p}, i}^2 \right]^2 \tag{28}$$

which gives an optimal solution $b = 2.28 \times 10^8 \ \mu\mathrm{m}/(\mathrm{V} \cdot \mathrm{s}^2)$. Nonetheless, this parameter will again be fine tuned later in the Monte Carlo process.
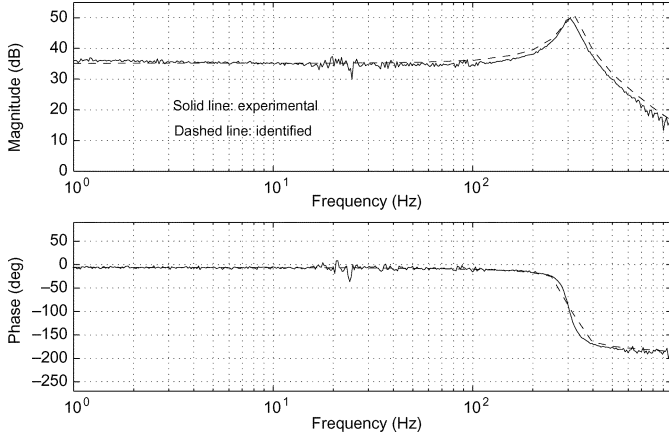
Fig. 6. Frequency response to small signals at the steady state with $u_0 = 0$.

Fig. 7. Frequency responses of the VCM actuator in the high-frequency region.

TABLE I
STATIC GAINS AND PEAK FREQUENCIES OF THE ACTUATOR FOR SMALL INPUTS

u_0 (mV)	$k_{\rm dc}$	$f_{\rm p}$ (Hz)
−10	60.73	310.30
−5	59.06	310.63
0	63.71	305.24
5	62.43	303.88
10	63.72	299.56
15	65.12	296.99
20	65.50	295.43

Lastly, we apply a Monte Carlo process to identify all other parameters of our VCM actuator model and to fine tune those parameters, which have previously been identified. Monte Carlo processes are known as numerical simulation methods, which make use of random numbers and probability statistics to solve some complicated mathematical problems. The detailed treatments of Monte Carlo methods vary widely from field to field. Originally, a Monte Carlo experiment means to use random numbers to examine some stochastic problems. The idea can be extended to deterministic problems by presetting some parameters and conditions of the problems. The use of Monte Carlo methods for modeling physical systems allows us to solve more complicated problems and provides approximate solutions to a variety of mathematical problems, whose analytical solutions are hard, if not impossible, to be derived. In what follows, a Monte Carlo process is utilized to obtain time-domain responses of the VCM actuator model in (18) with a set of presetting parameters $(b, a, c, d_0, d_1, d_2, d_3, d_4, d_5)$ and input signals. The corresponding frequency responses are obtained through Fourier transformation of the obtained time-domain responses. Our idea of using the Monte Carlo process is to minimize the differences between simulated frequency responses and the experimental ones by iteratively adjusting the parameters of the physical model in (18). The input signals in our simulations are again a combination of an offset u_0 and sinusoidal signals with a small amplitude 1 mV and several frequencies ranging from 1 Hz to 1 kHz.

Although Monte Carlo methods can only give locally minimal solutions, in our problem, however, the predetermined nonlinear characteristics of the data flex cable and the parameter b have given us a rough idea on what the true solution should be.
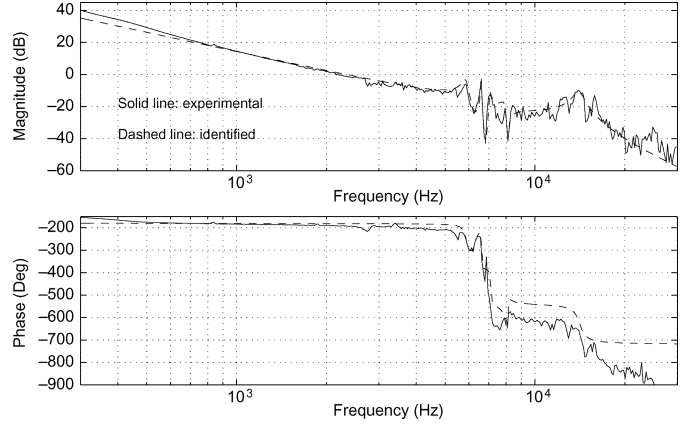
The solution within the neighborhood of the previously identified parameters are given by

$$\left.\begin{aligned}
b &= 2.35 \times 10^8 \ \mu{\rm m}/({\rm V} \cdot {\rm s}^2) \\
a &= 0.028\,87 \ {\rm V} \\
c &= 0.5886 \ (\mu{\rm m})^{-1} \\
d_0 &= 282.6 \ {\rm s}^{-1} \\
d_1 &= 0.005 \ (\mu{\rm m})^{-1} \\
d_2 &= 0.01 \ (\mu{\rm m})^{-1} \\
d_3 &= 1.5 \times 10^4 \ \mu{\rm m}/{\rm s}^2 \\
d_4 &= 0.0055 \ (\mu{\rm m})^{-1} \\
d_5 &= 1.65 \times 10^4 \ \mu{\rm m}/{\rm s}^2.
\end{aligned}\right\} \quad (29)$$

These parameters will be used for further verifications using the experimental setup of the actual system.

So far, we have only focused on the low-frequency components of the VCM actuator model. In fact, there are many high-frequency resonance modes, which are crucial to the overall performance of HDD servo systems. The high-frequency resonance modes of the VCM actuator can be obtained from frequency responses of the system in high-frequency region (see Fig. 7). The transfer function that matches the frequency responses given in Fig. 7 is identified using the standard least square estimation method [7] and is characterized by

$$G(s) = \frac{2.35 \times 10^8}{s^2} G_{\rm r.m.1}(s) G_{\rm r.m.2}(s) G_{\rm r.m.3}(s)$$
$$\times G_{\rm r.m.4}(s) G_{\rm r.m.5}(s) \quad (30)$$

with the resonance modes being given as

$$G_{\rm r.m.1}(s) = \frac{0.8709s^2 + 1726s + 1.369 \times 10^9}{s^2 + 1480s + 1.369 \times 10^9} \quad (31)$$

$$G_{\rm r.m.2}(s) = \frac{0.9332s^2 - 805.8s + 1.739 \times 10^9}{s^2 + 125.1s + 1.739 \times 10^9} \quad (32)$$

$$G_{\rm r.m.3}(s) = \frac{1.072s^2 + 925.1s + 1.997 \times 10^9}{s^2 + 536.2s + 1.997 \times 10^9} \quad (33)$$

$$G_{\rm r.m.4}(s) = \frac{0.9594s^2 + 98.22s + 2.514 \times 10^9}{s^2 + 1805s + 2.514 \times 10^9} \quad (34)$$

and

$$G_{\rm r.m.5}(s) = \frac{7.877 \times 10^9}{s^2 + 6212s + 7.877 \times 10^9}. \quad (35)$$
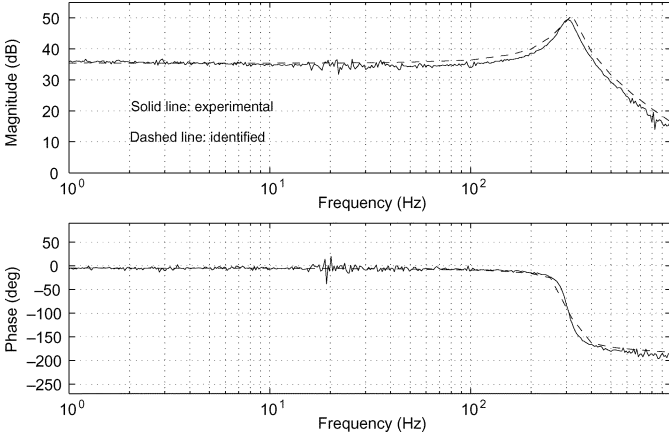
Fig. 8. Comparison of frequency responses to small signals of the VCM actuator with $u_0 = 5$ mV.

Fig. 9. Comparison of time-domain responses of the VCM actuator.

Finally, for easy reference, we conclude this section by explicitly expressing the identified rigid model of VCM actuator

$$\ddot{y} = 2.35 \times 10^8 u - 6.784\,45 \times 10^6 \arctan(0.5886y) + \tilde{T}_{\mathrm{f}} \quad (36)$$

where $T_f =$

$$\begin{cases} -\left[\left|1.175 \times 10^6 uy + 0.01(\dot{y})^2\right| \\ \quad +15\,000\right]\mathrm{sgn}(\dot{y}) - 282.6\dot{y}, & \dot{y} \neq 0, \\ -\tilde{T}_{\mathrm{e}}, & \dot{y} = 0, |\tilde{T}_{\mathrm{e}}| \leq \tilde{T}_{\mathrm{s}} \\ -\tilde{T}_{\mathrm{s}}\mathrm{sgn}(\tilde{T}_{\mathrm{e}}), & \dot{y} = 0, |\tilde{T}_{\mathrm{e}}| > \tilde{T}_{\mathrm{s}} \end{cases} \quad (37)$$

and where

$$\tilde{T}_{\mathrm{e}} = 2.35 \times 10^8 \left[-0.028\,87 \arctan(0.5886y) + u\right] \quad (38)$$

$$\tilde{T}_{\mathrm{s}} = 1.293 \times 10^6 |u_0 y_0| + 1.65 \times 10^4 \quad (39)$$

with u_0 and y_0 being, respectively, the corresponding input voltage and the displacement for the case when $\dot{y} = 0$. Note that in the previous model, the input signal u is in voltage and the output displacement y is in micrometer. Together with high-frequency resonance modes of (31)–(35), the previous model presents a fairly comprehensive characteristics of the VCM actuator studied. This model will be further verified using experimental tests on the actual system.

In order to verify the validity of the established model of the VCM actuator, we carry out a series of comparisons between the experimental results and computed results of the time-domain responses and frequency-domain responses of the actuator. The comparison of the frequency responses between experimental result and identified result for inputs consisting of $u_0 = 5$ mV and sine waves with amplitude of 1 mV is shown in Fig. 8. It clearly shows that the result of the identified model matches pretty well with the experimental result. The comparison of the time-domain responses for an input signal consisting of $u_0 = -5$ mV and a sine wave with an amplitude of 5 mV is given in Fig. 9. It shows that the simulation results match the trends and values of those obtained from experiments. The noises associated with experimental results in Figs. 8 and 9 are drift noises introduced by the LDV and/or DSA.

The comparisons of both frequency-domain and time-domain responses demonstrate that the identified model of the VCM actuator indeed describes the features of the actuator.
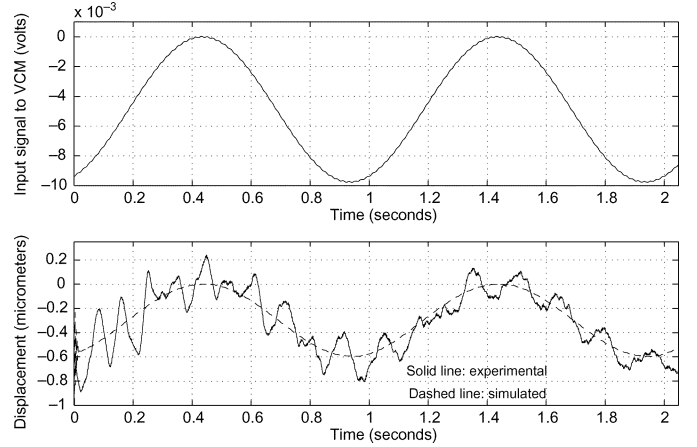
III. ENHANCED COMPOSITE NONLINEAR FEEDBACK CONTROL TECHNIQUE

We introduce in this section an enhanced version of the CNF control design, which is capable of removing constant bias in servo systems. The original CNF technique [7], [8], [20] is applicable to systems with input saturation but without external disturbances. It consists of two parts, the linear part and nonlinear part. The linear part is designed to yield a closed-loop system that has quick response, while at the same time not exceeding the actuator limits for the desired command input level. The nonlinear part is used to smooth out the overshoot caused by the linear part as the system output approaches the target reference. When the given system has disturbances, the resulting system output generally does not asymptotically match the target reference without knowing *a priori* the level of bias. A common approach for removing bias resulting from constant disturbances is to add an integrator to the controller. We propose in this section an enhanced CNF design scheme by introducing an additional integration action in the design. The new approach will retain the fast rise time property of the original CNF control and at the same time have an additional capacity of eliminating steady-state bias due to disturbances. We would like to note that there were attempts in the literature on improving tracking performance using modified proportional-integral derivative (PID) controllers [2], [25], [26] for certain classes of systems without input saturations. However, PID control is structure-wise very different from the CNF control technique considered in this work.

Specifically, we consider a linear system with an amplitude constrained actuator, characterized by

$$\begin{cases} \dot{x} = Ax + B\mathrm{sat}(u) + Ew, \ x(0) = x_0 \\ y = C_1 x \\ h = C_2 x \end{cases} \quad (40)$$

where $x \in \mathbb{R}^n$, $u \in \mathbb{R}$, $y \in \mathbb{R}^p$, $h \in \mathbb{R}$, and $w \in \mathbb{R}$ are, respectively, the state, control input, measurement output, controlled output, and disturbance input of the system. A, B, C_1, C_2, and E are appropriate dimensional constant matrices. The function, sat: $\mathbb{R} \rightarrow \mathbb{R}$, represents the actuator saturation defined as

$$\mathrm{sat}(u) = \mathrm{sgn}(u) \min \{u_{\max}, |u|\} \quad (41)$$

with $u_{\max}$ being the saturation level of the input. The assumptions on the given system are made:

1) (A, B) is stabilizable;
2) (A, C_1) is detectable;
3) (A, B, C_2) is invertible with no invariant zero at $s = 0$;
4) w is bounded unknown constant disturbance;
5) h is a subset of y, i.e., h is also measurable.

Note that all these assumptions are fairly standard for tracking control. We aim to design an enhanced CNF control law for the system with disturbances such that the resulting controlled output would track a target reference (set point), say r, as fast and as smooth as possible without having steady-state error. We first follow the usual practice to augment an integrator into the given system. Such an integrator will eventually become part of the final control law. To be more specific, we define an auxiliary state variable

$$\dot{x}_{\mathrm{i}} := \kappa_{\mathrm{i}}e := \kappa_{\mathrm{i}}(h - r) = \kappa_{\mathrm{i}}C_2 x - \kappa_{\mathrm{i}}r \qquad (42)$$

which is implementable as h is assumed to be measurable, and κ_{i} is a positive scalar to be selected to yield an appropriate integration action. The augmented system is then given as follows:

$$\begin{cases} \dot{\bar{x}} = \bar{A}\bar{x} + \bar{B}\mathrm{sat}(u) + \bar{B}_{\mathrm{r}}r + \bar{E}w \\ \bar{y} = \bar{C}_1\bar{x} \\ h = \bar{C}_2\bar{x} \end{cases} \qquad (43)$$

where

$$\bar{x} = \begin{pmatrix} x_{\mathrm{i}} \\ x \end{pmatrix} \quad \bar{x}_0 = \begin{pmatrix} 0 \\ x_0 \end{pmatrix} \quad \bar{y} = \begin{pmatrix} x_{\mathrm{i}} \\ y \end{pmatrix} \qquad (44)$$

$$\bar{A} = \begin{bmatrix} 0 & \kappa_{\mathrm{i}}C_2 \\ 0 & A \end{bmatrix} \quad \bar{B} = \begin{bmatrix} 0 \\ B \end{bmatrix} \quad \bar{B}_{\mathrm{r}} = \begin{bmatrix} -\kappa_{\mathrm{i}} \\ 0 \end{bmatrix} \qquad (45)$$

and

$$\bar{E} = \begin{bmatrix} 0 \\ E \end{bmatrix} \quad \bar{C}_1 = \begin{bmatrix} 1 & 0 \\ 0 & C_1 \end{bmatrix} \quad \bar{C}_2 = [0 \quad C_2]. \qquad (46)$$

It is straightforward to show that Assumptions 1 and 3 imply that the pair $(\bar{A}, \bar{B})$ is stabilizable.

Next, we proceed to carry out the design of enhanced CNF control laws for two different cases, i.e., the state feedback case and the reduced order measurement feedback case. The full order measurement feedback case is straightforward once the result for the reduced order case is established. We note that the procedure for designing the enhanced CNF control laws is a natural extension of that of [7], [8]. The enhanced control laws are, however, capable of removing steady-state bias.

A. State Feedback Case

We first investigate the case when all the state variables of the plant (43) are measurable, i.e., $\bar{y} = \bar{x}$. The procedure that generates an enhanced CNF state feedback law will be done in three steps. That is, in the first step, a linear feedback control law will be designed, in the second step, the design of nonlinear feedback control will be carried out, and lastly, in the final step, the linear and nonlinear feedback laws will be combined to form an enhanced CNF control law.

1) Design a linear feedback control law

$$u_{\mathrm{L}} = F\bar{x} + Gr \qquad (47)$$

where F is chosen such that 1) $\bar{A} + \bar{B}F$ is an asymptotically stable matrix, and 2) the closed-loop system $\bar{C}_2(sI - \bar{A} - \bar{B}F)^{-1}\bar{B}$ has certain desired properties. Let us partition $F = [F_{\mathrm{i}}\ F_{\mathrm{x}}]$ in conformity with x_{i} and x. The general guideline in design such an F is to place the closed-loop pole of $\bar{A} + \bar{B}F$ corresponding to the integration mode x_{i} to be sufficiently closer to the imaginary axis compared to the rest eigenvalues, which implies that F_{i} is a relatively small scalar. The remaining closed-loop poles of $\bar{A} + \bar{B}F$ should be placed to have a dominating pair with a small damping ratio, which in turn would yield a fast rise time in the closed-loop system response. Finally, G is chosen as

$$G = -\left[C_2(A + BF_{\mathrm{x}})^{-1}B\right]^{-1} \qquad (48)$$

which is well defined as (A, B, C_2) is assumed to have no invariant zeros at $s = 0$ and $A + BF_{\mathrm{x}}$ is nonsingular whenever $\bar{A} + \bar{B}F$ is stable and F_{i} is relatively small.

2) Given a positive–definite matrix $W \in \mathbb{R}^{(n+1)\times(n+1)}$, we solve the following Lyapunov equation:

$$(\bar{A} + \bar{B}F)'P + P(\bar{A} + \bar{B}F) = -W \qquad (49)$$

for $P > 0$. Such a solution is always existent as $\bar{A} + \bar{B}F$ is asymptotically stable. The nonlinear feedback portion of the enhanced CNF control law u_{N} is given by

$$u_{\mathrm{N}} = \rho(e)\bar{B}'P(\bar{x} - \bar{x}_{\mathrm{e}}) \qquad (50)$$

where $\rho(e)$, with $e = h - r$ being the tracking error, is a smooth and nonpositive function of $|e|$, and tends to a constant as $t \to \infty$. It is used to gradually change the system closed-loop damping ratio to yield a better tracking performance. The choices of the design parameters $\rho(e)$ and W will be discussed later. Next, we define

$$G_{\mathrm{e}} := \begin{bmatrix} 0 \\ -(A + BF_{\mathrm{x}})^{-1}BG \end{bmatrix} \quad \text{and} \quad \bar{x}_{\mathrm{e}} := G_{\mathrm{e}}r. \qquad (51)$$

3) The linear feedback control law and nonlinear feedback portion derived in the previous steps are now combined to form an enhanced CNF control law

$$u = u_{\mathrm{L}} + u_{\mathrm{N}} = F\bar{x} + Gr + \rho(e)\bar{B}'P(\bar{x} - \bar{x}_{\mathrm{e}}). \qquad (52)$$

We have the following result.

Theorem 1: Consider the given system (40) with $y = x$ and the disturbance w being bounded by a nonnegative scalar τ_w, i.e., $|w| \leq \tau_w$. Let

$$\gamma := 2\tau_w \lambda_{\max}(PW^{-1})(\bar{E}'P\bar{E})^{\frac{1}{2}}. \qquad (53)$$

Then, for any $\rho(e)$, which is a smooth and nonpositive function of $|e|$ and tends to a constant as $t \to \infty$, the enhanced CNF control law (52) will drive the system controlled output h to track

the step reference of amplitude r from an initial state $\bar{x}_0$ asymptotically without steady-state error, provided that the following conditions are satisfied.

1) There exist positive scalars $\delta \in (0, 1)$ and $c_\delta > \gamma^2$ such that

$$\forall \bar{x} \in \boldsymbol{X}(F, c_\delta) := \{\bar{x} : \bar{x}'P\bar{x} \le c_\delta\}$$
$$\Rightarrow |F\bar{x}| \le (1 - \delta)u_{\max}. \tag{54}$$

2) The initial condition $\bar{x}_0$ satisfies

$$\bar{x}_0 - \bar{x}_e \in \boldsymbol{X}(F, c_\delta). \tag{55}$$

3) The level of the target reference, r, satisfies

$$|Hr| \le \delta u_{\max} \tag{56}$$

where $H := FG_e + G$.

Proof: For simplicity, we drop the variable e in $\rho(e)$ throughout this proof. Noting that

$$\bar{A}\bar{x}_e + \bar{B}Hr + \bar{B}_r r$$
$$= \bar{A}\bar{x}_e + \bar{B}(FG_e + G)r + \bar{B}_r r$$
$$= (\bar{A} + \bar{B}F)\bar{x}_e + \bar{B}_r r + \bar{B}Gr$$
$$= \begin{bmatrix} 0 & \kappa_i C_2 \\ BF_i & A + BF_x \end{bmatrix} \begin{bmatrix} 0 \\ -(A + BF_x)^{-1}BG \end{bmatrix} r$$
$$+ \begin{bmatrix} -\kappa_i \\ 0 \end{bmatrix} r + \begin{bmatrix} 0 \\ BG \end{bmatrix} r$$
$$= \begin{bmatrix} -\kappa_i C_2(A + BF_x)^{-1}BG \\ -BG \end{bmatrix} r + \begin{bmatrix} -\kappa_i \\ BG \end{bmatrix} r$$
$$= 0 \tag{57}$$

and letting $\tilde{x} = \bar{x} - \bar{x}_e$, then the dynamics equation of the augmented plant in (43) can be expressed as

$$\dot{\tilde{x}} = \dot{\bar{x}} = \bar{A}(\tilde{x} + \bar{x}_e) + \bar{B}\mathrm{sat}(u) + \bar{B}_r r + \bar{E}w$$
$$= (\bar{A} + \bar{B}F)\tilde{x} + \bar{A}\bar{x}_e - \bar{B}F\tilde{x} + \bar{B}\mathrm{sat}(u) + \bar{B}_r r + \bar{E}w$$
$$= (\bar{A} + \bar{B}F)\tilde{x} + \bar{B}[\mathrm{sat}(u) - F\tilde{x} - Hr]$$
$$\quad + (\bar{A}\bar{x}_e + \bar{B}Hr + \bar{B}_r r) + \bar{E}w$$
$$= (\bar{A} + \bar{B}F)\tilde{x} + \bar{B}v + \bar{E}w \tag{58}$$

where $v := \mathrm{sat}(u) - F\tilde{x} - Hr$. Following the similar lines of reasoning as those in [8], we can show that for $\tilde{x} \in \boldsymbol{X}(F, c_\delta)$ and $|Hr| \le \delta u_{\max}$, v can be expressed as $v = q\rho\bar{B}'P\tilde{x}$, for some nonnegative variable $q \in [0, 1]$. Thus, for the case when $\tilde{x} \in \boldsymbol{X}(F, c_\delta)$ and $|Hr| \le \delta u_{\max}$, the closed-loop system comprising the given augmented plant (43) and the enhanced CNF control law (52) can be expressed as the following:

$$\dot{\tilde{x}} = (\bar{A} + \bar{B}F + q\rho\bar{B}\bar{B}'P)\tilde{x} + \bar{E}w. \tag{59}$$

In what follows, we will show that (59) is stable provided that the initial condition, $\bar{x}_0$, the target reference, r, and the disturbance, w, satisfy those conditions listed in the theorem. Let us

define a Lyapunov function $V = \tilde{x}'P\tilde{x}$. For easy derivation, we introduce a matrix S such that $P = S'S$. We then obtain the derivative of V calculated along the trajectory of the system (59)

$$\dot{V} = \dot{\tilde{x}}'P\tilde{x} + \tilde{x}'P\dot{\tilde{x}}$$
$$= \tilde{x}'\left[(\bar{A} + \bar{B}F)'P + P(\bar{A} + \bar{B}F)\right]\tilde{x} + 2q\rho\tilde{x}'P\bar{B}\bar{B}'P\tilde{x}$$
$$\quad + 2\tilde{x}'P\bar{E}w$$
$$\le -\tilde{x}'W\tilde{x} + 2\tilde{x}'P\bar{E}w$$
$$= -\tilde{x}'S'SP^{-1}WP^{-1}S'S\tilde{x} + 2\tilde{x}'S'S\bar{E}w$$
$$\le -\lambda_{\min}(SP^{-1}WP^{-1}S')\tilde{x}'S'S\tilde{x} + 2\|S\tilde{x}\| \cdot \|S\bar{E}'\|\tau_w$$
$$= -\lambda_{\min}(P^{-1}W)\tilde{x}'P\tilde{x} + 2\tau_w(\tilde{x}'P\tilde{x})^{\frac{1}{2}}(\bar{E}'P\bar{E})^{\frac{1}{2}}$$
$$= -\lambda_{\min}(P^{-1}W)(\tilde{x}'P\tilde{x})^{\frac{1}{2}}$$
$$\quad \times \left[(\tilde{x}'P\tilde{x})^{\frac{1}{2}} - 2\tau_w\lambda_{\max}(PW^{-1})(\bar{E}'P\bar{E})^{\frac{1}{2}}\right]$$
$$= -\lambda_{\min}(P^{-1}W)(\tilde{x}'P\tilde{x})^{\frac{1}{2}}\left[(\tilde{x}'P\tilde{x})^{\frac{1}{2}} - \gamma\right]. \tag{60}$$

We note that we have used the following matrix properties: 1) $z'Xz \ge \lambda_{\min}(X)z'z$, where X is a symmetric matrix; 2) $\lambda(XY) = \lambda(YX)$, if both X and Y are square matrices; and 3) $\lambda(XY) > 0$ if $X > 0$ and $Y > 0$. Clearly, the closed-loop system in the absence of the disturbance, w, has $\dot{V} < 0$ and, thus, is asymptotically stable.

With the presence of the disturbance, w, and with the initial condition $\tilde{x}(0) = \bar{x}_0 - \bar{x}_e \in \boldsymbol{X}(F, c_\delta)$, where $c_\delta > \gamma^2$, the corresponding trajectory of (59) will remain in $\boldsymbol{X}(F, c_\delta)$ and converge to a point on a ball $\{\tilde{x} : \tilde{x}'P\tilde{x} \le \tilde{\gamma}^2\}$ with $\tilde{\gamma} \le \gamma$. Since $x_i(t) = \int_0^t \kappa_i e(\tau)d\tau$ converges to a constant, it is clear that the tracking error $e(t) \to 0$ as $t \to \infty$. This completes the proof of Theorem 1.

B. Measurement Feedback Case

In practical situations, it is unrealistic to assume that all the state variables of a given plant to be measurable. In what follows, we will design an enhanced CNF control law using only information measurable from the plant. In principle, we can design either a full order measurement feedback control law, for which its dynamical order will be identical to that of the given plant, or a reduced order measurement feedback control law, in which we make a full use of the measurement output and estimate only the unknown part of the state variable. As such, the dynamical order of the controller will be reduced. It is more feasible to implement controllers with smaller dynamical order. The procedure in the following on the enhanced CNF control using reduced order measurement feedback follows pretty closely from that of [8].

For simplicity of presentation, we assume that C_1 in the measurement output of the given plant (40) is already in the form

$$C_1 = \begin{bmatrix} I_p & 0 \end{bmatrix}. \tag{61}$$

The augmented plant (43) can then be partitioned as the following:

$$
\begin{cases}
\begin{pmatrix} \dot{x}_i \\ \dot{x}_1 \\ \dot{x}_2 \end{pmatrix} = \begin{bmatrix} 0 & \kappa_i C_{21} & \kappa_i C_{22} \\ 0 & A_{11} & A_{12} \\ 0 & A_{21} & A_{22} \end{bmatrix} \begin{pmatrix} x_i \\ x_1 \\ x_2 \end{pmatrix} + \begin{bmatrix} 0 \\ B_1 \\ B_2 \end{bmatrix} \text{sat}(u) \\
\qquad + \begin{bmatrix} -\kappa_i \\ 0 \\ 0 \end{bmatrix} r + \begin{bmatrix} 0 \\ E_1 \\ E_2 \end{bmatrix} w \\
\bar{y} = \begin{bmatrix} 1 & 0 & 0 \\ 0 & I_p & 0 \end{bmatrix} \begin{pmatrix} x_i \\ x_1 \\ x_2 \end{pmatrix} \\
h = \begin{bmatrix} 0 & C_{21} & C_{22} \end{bmatrix} \begin{pmatrix} x_i \\ x_1 \\ x_2 \end{pmatrix}
\end{cases}
\tag{62}
$$

where

$$
\begin{pmatrix} x_i \\ x_1 \\ x_2 \end{pmatrix} = \bar{x} \quad \begin{pmatrix} x_i(0) \\ x_1(0) \\ x_2(0) \end{pmatrix} = \begin{pmatrix} 0 \\ x_{10} \\ x_{20} \end{pmatrix} = \bar{x}_0 \tag{63}
$$

and

$$
\bar{y} = \begin{pmatrix} x_i \\ y \end{pmatrix} = \begin{pmatrix} x_i \\ x_1 \end{pmatrix}. \tag{64}
$$

Clearly, x_i and x_1 are readily available and need not be estimated. We only need to estimate x_2. There are two main step in designing a reduced order measurement feedback control laws: 1) the construction of a full state feedback gain matrix F; and 2) the construction of a reduced order observer gain matrix K_R. The construction of the gain matrix F is totally identical to that given in the previous subsection, which can be partitioned in conformity with x_i, x_1 and x_2, as follows:

$$
F = [F_i \quad F_1 \quad F_2]. \tag{65}
$$

The reduced order observer gain matrix K_R is chosen such that the poles of $A_{22} + K_R A_{12}$ are placed in appropriate locations in the open-left half plane.

The reduced order enhanced CNF control law is then given by

$$
\dot{x}_v = (A_{22} + K_R A_{12})x_v + (B_2 + K_R B_1)\text{sat}(u) \\
\qquad + [A_{21} + K_R A_{11} - (A_{22} + K_R A_{12})K_R]y \tag{66}
$$

and

$$
u = F \begin{pmatrix} x_i \\ x_1 \\ x_v - K_R y \end{pmatrix} + Gr + \rho(e)\bar{B}'P \left[\begin{pmatrix} x_i \\ x_1 \\ x_v - K_R y \end{pmatrix} - \bar{x}_e \right] \tag{67}
$$

where G is as defined in (48) and $\rho(e)$ is the smooth, nonpositive, and nondecreasing function of $|e|$, to be chosen to yield a desired performance.

Next, given a positive–definite matrix $W \in \mathbb{R}^{(n+1)\times(n+1)}$, let $P > 0$ be the solution to the Lyapunov equation

$$
(\bar{A} + \bar{B}F)'P + P(\bar{A} + \bar{B}F) = -W. \tag{68}
$$

Given another positive–definite matrix $W_R \in \mathbb{R}^{(n-p)\times(n-p)}$ with

$$
W_R > F_2'\bar{B}'PW^{-1}P\bar{B}F_2 \tag{69}
$$

let $Q_R > 0$ be the solution to the Lyapunov equation

$$
(A_{22} + K_R A_{12})'Q_R + Q_R(A_{22} + K_R A_{12}) = -W_R. \tag{70}
$$

Note that such P and Q_R exist as $\bar{A} + \bar{B}F$ and $A_{22} + K_R A_{12}$ are both asymptotically stable. We have the following result.

Theorem 2: Consider the given system (40) with the disturbance w being bounded by a nonnegative scalar τ_w, i.e., $|w| \leq \tau_w$. Let

$$
\gamma_R := 2\tau_w \lambda_{\max} \left(\begin{bmatrix} P & 0 \\ 0 & Q_R \end{bmatrix} \begin{bmatrix} W & -P\bar{B}F_2 \\ -F_2'\bar{B}'P & W_R \end{bmatrix}^{-1} \right) \\
\times [\bar{E}'P\bar{E} + (E_2 + K_R E_1)'Q_R(E_2 + K_R E_1)]^{\frac{1}{2}}. \tag{71}
$$

Then, there exists a scalar $\rho^* > 0$ such that for any $\rho(e)$, a smooth and nonpositive function of $|e|$ with $|\rho(e)| \leq \rho^*$, the enhanced reduced order CNF control law of (66) and (67) will drive the system controlled output h to track the step reference of amplitude r asymptotically without steady-state error, provided that the following conditions are satisfied:

1) There exist positive scalars $\delta \in (0,1)$ and $c_{R\delta} > \gamma_R^2$ such that

$$
\forall \bar{x} \in \boldsymbol{X}(F, c_{R\delta}) := \left\{ \bar{x} : \bar{x}' \begin{bmatrix} P & 0 \\ 0 & Q_R \end{bmatrix} \bar{x} \leq c_{R\delta} \right\} \\
\Rightarrow |[F \quad F_2]\bar{x}| \leq (1-\delta)u_{\max}. \tag{72}
$$

2) The initial conditions, $\bar{x}_0$ and $x_{v0} = x_v(0)$, satisfy

$$
\begin{pmatrix} \bar{x}_0 - \bar{x}_e \\ x_{v0} - x_{20} - K_R x_{10} \end{pmatrix} \in \boldsymbol{X}(F, c_{R\delta}). \tag{73}
$$

3) The level of the target reference r satisfies

$$
|Hr| \leq \delta u_{\max} \tag{74}
$$

where H is the same as that defined in Theorem 1.

Proof: The result follows from similar lines of reasoning as those given in Theorem 1 and those for the measurement feedback case in [8].

C. Selection of W and the Nonlinear Gain $\rho(e)$

The procedures for selecting the design parameter W and the nonlinear gain $\rho(e)$ for the enhanced CNF control laws are the same as those for the usual CNF design given in [8]. We recall in the following the selection procedures for W and $\rho(e)$ from [8] for completeness. Basically, the freedom to choose the function $\rho(e)$ is used to tune the control laws so as to improve the performance of the closed-loop system as the controlled output h approaches the set point, r. Since the main purpose of adding the nonlinear part to the CNF or the enhanced CNF controllers is to
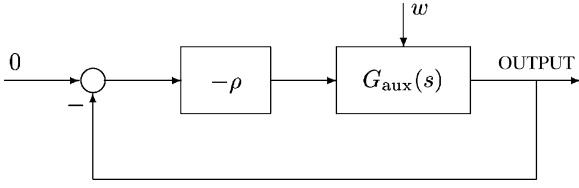
Fig. 10.   Interpretation of the nonlinear function $\rho(e)$.

Fig. 11.   Control scheme for the HDD servo system.

speed up the settling time, or equivalently to contribute a significant value to the control input when the tracking error e is small. The nonlinear part, in general, will be set in action when the control signal is far away from its saturation level and, thus, it will not cause the control input to hit its limits. Under such a circumstance, the closed-loop system comprising the augmented plant in (43) and the enhanced CNF control law can be expressed as

$$\dot{\tilde{x}} = (\bar{A} + \bar{B}F + \rho\bar{B}\bar{B}'P)\tilde{x} + \bar{E}w. \tag{75}$$

We note that the additional term $\rho(e)$ does not affect the stability of the estimators. It is now clear that eigenvalues of the closed-loop system in (75) can be changed by the function $\rho(e)$. Such a mechanism can be interpreted using the classical feedback control concept as shown in Fig. 10, where the auxiliary system $G_{\mathrm{aux}}(s)$ is defined as

$$\begin{aligned} G_{\mathrm{aux}}(s) &:= C_{\mathrm{aux}}(sI - A_{\mathrm{aux}})^{-1}B_{\mathrm{aux}} \\ &:= \bar{B}'P(sI - \bar{A} - \bar{B}F)^{-1}\bar{B}. \end{aligned} \tag{76}$$

Following the result of [8], we can show that $G_{\mathrm{aux}}(s)$ is stable and invertible with a relative degree equal to 1, and is of minimum phase with n stable invariant zeros.

The invariant zeros of $G_{\mathrm{aux}}(s)$ play an important role in selecting the poles of the closed-loop system of (75). The poles of the closed-loop system approach the locations of the invariant zeros of $G_{\mathrm{aux}}(s)$ as $|\rho|$ becomes larger and larger. We would like to note that there is freedom in preselecting the locations of these invariant zeros. This can actually be done by selecting an appropriate $W > 0$. In general, we can employ the result of Chen and Zheng [9] on finite and infinite zero assignment to select the invariant zeros of $G_{\mathrm{aux}}(s)$, which are corresponding to the closed-loop poles for larger $|\rho|$, such that the dominating ones have a large damping ratio, which in turn will yield a smaller overshoot. We refer interested readers to [8].

The selection of the nonlinear function $\rho(e)$ is relatively simple once the desired invariant zeros of $G_{\mathrm{aux}}(s)$ are obtained. The following choice of $\rho(e)$ is a smooth and nonpositive function of $|e|$

$$\rho(e) = -\beta\left|e^{-\alpha|e|} - e^{-\alpha|h(0)-r|}\right| \tag{77}$$

where α and β are appropriate positive scalars that can be chosen to yield a desired performance, i.e., fast settling time and small overshoot. This function $\rho(e)$ changes from 0 to $\rho_0 = -\beta|1 - e^{-\alpha|h(0)-r|}|$ as the tracking error approaches zero. At the initial stage, when the controlled output h is far away from the final set point, $\rho(e)$ is small and the effect of the nonlinear part on the overall system is very limited. When
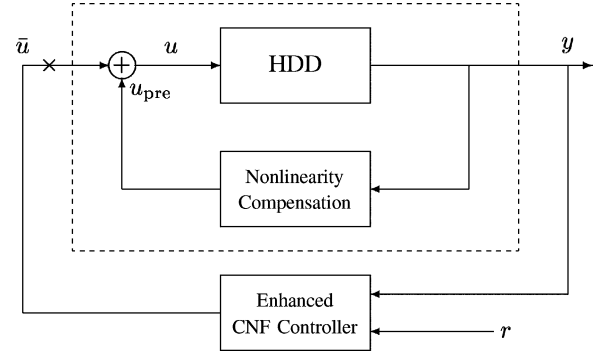
the controlled output, h, approaches the set point, $\rho(e) \approx \rho_0$, and the nonlinear control law will become effective. In general, the parameter ρ_0 should be chosen such that the poles of $\bar{A} + \bar{B}F + \rho_0\bar{B}\bar{B}'P$ are in the desired locations, e.g., the dominated poles should have a large damping ratio, which would reduce the overshoot of the output response. Note that the choice of $\rho(e)$ is nonunique. Any function would work so long as it has similar properties of that given in (77). Finally, we also note that the CNF control technique reported in this section has recently been implemented in MATLAB, which is available for free at http://hdd.ece.nus.edu.sg/~bmchen.

IV. MICRODRIVE SERVO SYSTEM DESIGN

We proceed to design a servo system for the microdrive identified in Section II. As mentioned earlier, our design philosophy is rather simple. We will make a full use of the obtained model of the friction and nonlinearities of the VCM actuator to design a precompensator, which would cancel as much as possible all the unwanted elements in the servo system. As it is impossible to have perfect models for friction and nonlinearities, a perfect cancellation of these elements is unlikely to happen in the real world. We will then formulate our design by treating the uncompensated portion as external disturbances. The enhanced CNF control technique of Section III will then be employed to design an effective tracking controller. The overall control scheme for the servo system is depicted in Fig. 11. Although we focus our attention here on HDD, it is our belief that such an approach can be adopted to solve other servo problems.

Examining the model of (36), it is easy to obtain a precompensation

$$u_{\mathrm{pre}} = u - \bar{u} = 0.028\,873\,7\arctan(0.5886y) \tag{78}$$

which would eliminate the majority of nonlinearities in the data flex cable. The HDD model of (18) can then be simplified as the following:

$$\begin{cases} \dot{x} = \begin{bmatrix} 0 & 1 \\ 0 & 0 \end{bmatrix} x + \begin{bmatrix} 0 \\ 2.35 \times 10^8 \end{bmatrix}[\mathrm{sat}(\bar{u}) + w] \\ y = h = \begin{bmatrix} 1 & 0 \end{bmatrix}x \end{cases} \tag{79}$$

where the disturbance w represents uncompensated nonlinearities, and $y = h$ is the relative displacement of the R/W head (in micrometer). The control input $\bar{u}$ is to be limited within $\pm\bar{u}_{\mathrm{max}}$

with $\bar{u}_{\max} = 3$ V. Letting $\kappa_i = 1$, we obtain the corresponding augmented plant to be used in the enhanced CNF design

$$
\begin{cases}
\dot{\bar{x}} = \begin{bmatrix} 0 & 1 & 0 \\ 0 & 0 & 1 \\ 0 & 0 & 0 \end{bmatrix} \bar{x} + \begin{bmatrix} 0 \\ 0 \\ 2.35 \times 10^8 \end{bmatrix} \text{sat}(\bar{u}) \\
\quad + \begin{bmatrix} -1 \\ 0 \\ 0 \end{bmatrix} r + \begin{bmatrix} 0 \\ 0 \\ 2.35 \times 10^8 \end{bmatrix} w \\
y = h = \begin{bmatrix} 0 & 1 & 0 \end{bmatrix} \bar{x}.
\end{cases}
\tag{80}
$$

We will focus on our design for $r = 1$ in this section, i.e., the track following stage of the HDD servo system. The initial state $x(0)$ is assumed to be 0. Note that the nonlinearities in the data flex cable and friction do not cause much trouble in the track seeking stage.

Following the procedures given in Section III and few simulation tries, we obtain a state feedback gain matrix

$$
F = -\begin{bmatrix} 8.2317 \times 10^{-4} & 0.0823 & 2.2459 \times 10^{-5} \end{bmatrix} \tag{81}
$$

which places the poles of $\bar{A} + \bar{B}F$ at $-2638.9 \pm j3518.6$ and -0.01, and which work very well for the HDD servo system. Next, we choose W to be a diagonal matrix with diagonal elements being 7.4536×10^{-4}, 0.0135, and 7.0057×10^{-11}, respectively. Solving the Lyapunov equation of (49), we obtain

$$
P = \begin{bmatrix} 0.0373 & 1.0182 \times 10^{-5} & 1.9266 \times 10^{-9} \\ 1.0182 \times 10^{-5} & 3.2591 \times 10^{-6} & 3.5028 \times 10^{-10} \\ 1.9266 \times 10^{-9} & 3.5028 \times 10^{-10} & 7.3005 \times 10^{-14} \end{bmatrix}
$$

which is indeed positive–definite. The reduced order observer gain matrix is selected as

$$
K_R = -6000 \tag{82}
$$

which places the observer pole at -6000, and the nonlinear gain function is selected as follows:

$$
\rho(e) = -4.7459 \left| e^{-|e|} - 0.3679 \right|. \tag{83}
$$

Finally, the reduced order enhanced CNF control law for the microdrive servo system is given by

$$
\begin{pmatrix} \dot{x}_i \\ \dot{x}_v \end{pmatrix} = \begin{bmatrix} 0 & 0 \\ 0 & -6000 \end{bmatrix} \begin{pmatrix} x_i \\ x_v \end{pmatrix} + \begin{bmatrix} 1 \\ -3.6 \times 10^7 \end{bmatrix} y
$$
$$
\quad + \begin{bmatrix} 0 \\ 2.35 \times 10^8 \end{bmatrix} \text{sat}(\bar{u}) - \begin{bmatrix} 1 \\ 0 \end{bmatrix} r \tag{84}
$$

and

$$
\bar{u} = \left(-\begin{bmatrix} 8.2317 \times 10^{-4} & 0.0823 & 2.2459 \times 10^{-5} \end{bmatrix} + \rho(e) \right.
$$
$$
\left. \times \begin{bmatrix} 0.4527 & 0.0823 & 1.7156 \times 10^{-5} \end{bmatrix} \right) \begin{pmatrix} x_i \\ y - r \\ x_v + 6000y \end{pmatrix}. \tag{85}
$$

To see the effectiveness of the nonlinearity compensation, we design a normal reduced order CNF control law using the tech-
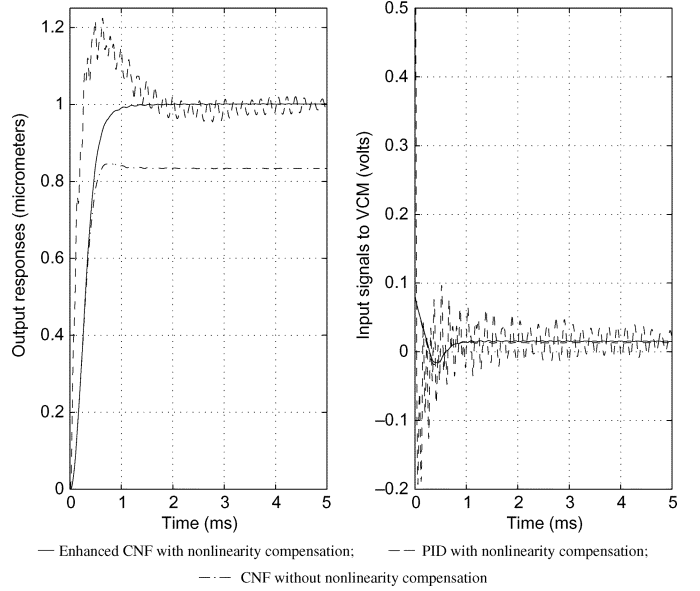

Fig. 12. Servo performance (simulation results).

nique reported in [8] for the original plant without the precompensation, which is given by

$$
\dot{x}_v = -6000x_v - 3.6 \times 10^7 y + 2.35 \times 10^8 \text{sat}(u) \tag{86}
$$

and

$$
u = \left(-\begin{bmatrix} 0.0823 & 2.2459 \times 10^{-5} \end{bmatrix} \right.
$$
$$
\left. + \rho(e)\begin{bmatrix} 0.0823 & 1.7156 \times 10^{-5} \end{bmatrix} \right) \begin{pmatrix} y - r \\ x_v + 6000y \end{pmatrix} \tag{87}
$$

where $\rho(e)$ is the same as in (83).

To compare the result of the enhanced CNF technique with conventional approaches, we design a conventional PID controller for the precompensated system

$$
\bar{u} = -\left(k_p + \frac{k_d s}{\frac{T s}{N} + 1} + \frac{k_i}{s} \right) e \tag{88}
$$

where T is the sampling period used in implementation and N is a sufficiently large positive scalar to be selected for the approximation of the derivative action. The parameters in (88) are tuned to yield the best possible implementation result under this control structure, which are given as

$$
T = 10^{-4} \text{ s} \quad N = 10 \tag{89}
$$

and

$$
k_p = 0.0605 \quad k_d = 2.8876 \times 10^{-5} \quad k_i = 50. \tag{90}
$$

For simulation, we use the nonlinear model of the HDD in (36) together with all its identified resonance modes given in (31)–(35). The simulations are done in a continuous setting, and $|\dot{y}| \leq 0.01$ μm/s is considered to be 0. The simulation results are shown in Fig. 12. Experiments are done on the actual HDD with its cover being removed. The HDD is placed on a vibration-
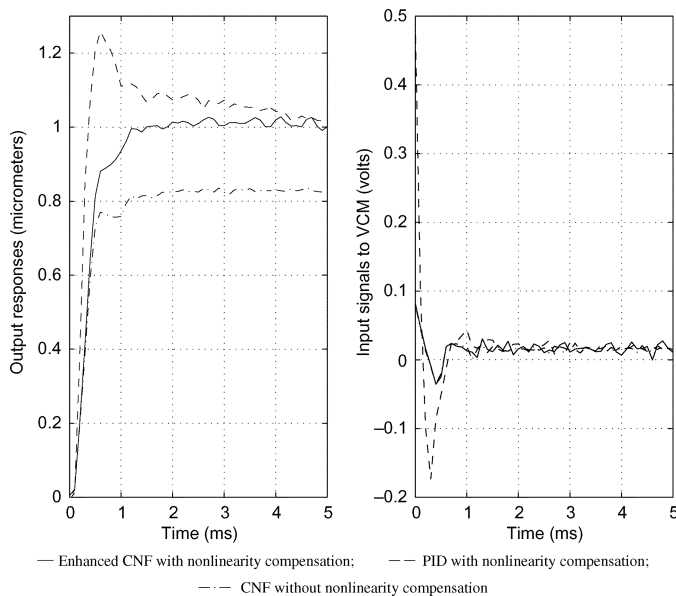
Fig. 13.   Servo performance (experimental results).

TABLE II
SETTLING TIME: ENHANCED CNF CONTROL VERSUS PID CONTROL

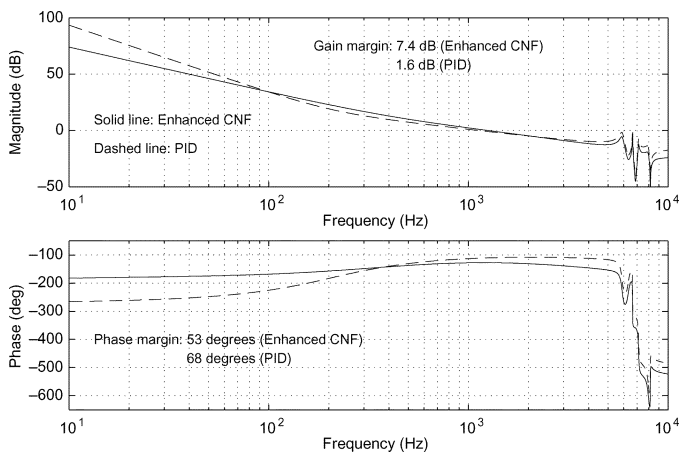| Controller	PID	CNF	Improvement
Simulation	1.7 ms	0.8 ms	53%
Implementation	4.5 ms	1.1 ms	76%

Fig. 14.   Frequency responses of the open-loop systems.

free platform and the LDV with a resolution set to 10 nm is used to measure the displacement of the R/W head of the HDD. The controllers are implemented using a dSpace DSP installed in a desktop computer. The sampling frequency is set to be 10 kHz, a typical sampling frequency used in HDD servo systems. The experimental results are shown in Fig. 13. We summarize in Table II the tracking performances in terms of 3% settling time, which is within 5% of the track-width for 40 kTPI (kilo-tracks per inch) drives. Clearly, the performance of the enhanced CNF control is much better than that of the PID control.

We next examine the frequency domain properties of the servo system by breaking the loop at the input point to the pre-compensated plant (marked "×" in Fig. 11) and computing its

open-loop frequency response with a multiplication of -1 for negative unit feedback and with the reference input, r, being set to 0. For the CNF control, which is nonlinear, we replace $\rho(e)$ by $\rho_0 = -3$, representing the steady-state situation of such a control scheme. The resulting frequency responses of the servo system shown in Fig. 14 clearly indicate that the servo system with the enhanced CNF controller has a gain margin of 7.4 dB (at the phase crossover frequency around 5734 Hz) and a phase margin of 53° (at the gain crossover frequency around 1250 Hz), while the one with the PID controller has a gain margin of 1.6 dB (at the phase crossover frequency around 5861 Hz) and a phase margin of 68° (at the gain crossover frequency around 1124 Hz). The gain margin in the PID control is not acceptable in practical situations. This could be due to the fact that we have tuned the response of the PID control a bit too fast, although it is very slow compared to that of the enhanced CNF control.

V. CONCLUDING REMARKS

We have identified in this paper fairly comprehensive features of friction and nonlinearities for a typical VCM actuator used in an IBM microdrive. It has been done through the detailed analysis of physical effects of components that make up the actuator, i.e., the coil, R/W head, pivot bearing and data flex cable. The verification of the identified model shows it indeed describes the features of the friction and nonlinearities of the actuator. A control structure with a nonlinearity precompensation and an enhanced composite nonlinear feedback control technique has then been developed and utilized to design a servo system for the microdrive. The simulation and implementation results show that our approach is very efficient and successful. Such a method can be adopted to solve servomechanism problems.

REFERENCES

[1] D. Abramovitch, F. Wang, and G. Franklin, "Disk drive pivot nonlinearity modeling part I: frequency domain," in Proc. Amer. Control Conf., Baltimore, MD, 1994, pp. 2600–2603.
[2] B. Armstrong, D. Neevel, and T. Kusik, "New results in NPID control: tracking, integral control, friction compensation and experimental results," IEEE Trans. Contr. Syst. Technol., vol. 9, pp. 399–406, 2001.
[3] C. Canudas de Wit and P. Lischinsky, "Adaptive friction compensation with partially known dynamic friction model," Int. J. Adapt. Control Signal Process., vol. 11, pp. 65–80, 1997.
[4] C. Canudas de Wit, H. Olsson, K. J. Astrom, and P. Lischinsky, "A new model for control of systems with friction," IEEE Trans. Autom. Control, vol. 40, pp. 419–425, 1995.
[5] C. Canudas de Wit, H. Olsson, K. J. Astrom, and P. Lischinsky, "Dynamic friction models and control design," in Proc. Amer. Control Conf., San Francisco, CA, 1993, pp. 1920–1926.
[6] H. S. Chang, S. E. Baek, J. H. Park, and Y. K. Byun, "Modeling of pivot friction using relay function and estimation of its functional parameters," in Proc. Amer. Control Conf., San Francisco, CA, 1999, pp. 3784–3789.
[7] B. M. Chen, T. H. Lee, and V. Venkataramanan, Hard Disk Drive Servo Systems.   New York: Springer-Verlag, 2002.
[8] B. M. Chen, T. H. Lee, K. Peng, and V. Venkataramanan, "Composite nonlinear feedback control: theory and an application," IEEE Trans. Autom. Control, vol. 48, no. 3, pp. 427–439, Mar. 2003.
[9] B. M. Chen and D. Z. Zheng, "Simultaneous finite and infinite zero assignments of linear systems," Automatica, vol. 31, pp. 643–648, 1995.
[10] P. R. Dahl, "Solid friction damping of mechanical vibrations," AIAA J., vol. 14, pp. 1675–1682, 1976.
[11] D. Dammers, P. Binet, G. Pelz, and L. M. Vobkarper, "Motor modeling based on physical effect models," in Proc. IEEE Int. Workshop Behavioral Modeling and Simulation, Santa Rosa, CA, 2001, pp. 78–83.
[12] A. Dubi, Monte Carlo Applications in Systems Engineering.   New York: Wiley, 2000.

[13] M. Evans and T. Swartz, *Approximating Integrals via Monte Carlo and Deterministic Methods*. Oxford, U.K.: Oxford Univ. Press, 2000.

[14] P. Eykhoff, *System Identification—Parameter and State Estimation*. New York: Wiley, 1981.

[15] G. F. Franklin, J. D. Powell, and M. L. Workman, *Digital Control of Dynamic Systems*. Reading, MA: Addison-Wesley, 1990.

[16] S. S. Ge, T. H. Lee, and S. X. Ren, "Adaptive friction compensation of servomechanisms," *Int. J. Syst. Sci.*, vol. 32, pp. 523–532, 2001.

[17] J. Q. Gong, L. Guo, H. S. Lee, and B. Yao, "Modeling and cancellation of pivot nonlinearity in hard disk drives," *IEEE Trans. Magn.*, vol. 38, pp. 3560–3565, 2002.

[18] J. Ishikawa and M. Tomizuka, "A novel add-on compensator for cancellation of pivot nonlinearities in hard disk drives," *IEEE Trans. Magn.*, vol. 34, pp. 1895–1897, 1998.

[19] ——, "Pivot friction compensation using an accelerometer and a disturbance observer for hard disk drives," *IEEE/ASME Trans. Mechatronics*, vol. 3, pp. 194–201, 1998.

[20] Z. Lin, M. Pachter, and S. Banda, "Toward improvement of tracking performance—nonlinear feedback for linear system," *Int. J. Control*, vol. 70, pp. 1–11, 1998.

[21] X. Liu and J. C. Liu, "Analysis and measurement of torque hysteresis of pivot bearing in hard disk drive applications," *Tribology Int.*, vol. 32, pp. 125–130, 1999.

[22] H. A. Maria and I. D. Abrahams, "Active control of friction-driven oscillations," *J. Sound Vib.*, vol. 193, pp. 417–426, 1996.

[23] G. A. Mikhailov, *Parametric Estimates by the Monte Carlo Method*. Utrecht, The Netherlands: V.S.P. International Science, 1999.
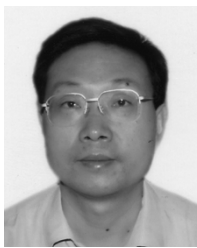
[24] H. Olsson and K. J. Astrom, "Observer-based friction compensation," in *Proc. 35th IEEE Conf. Decision and Control*, Kobe, Japan, 1996, pp. 4345–4350.

[25] H. Seraji, "Nonlinear and adaptive control of force and compliance in manipulators," *Int. J. Robot. Res.*, vol. 17, pp. 467–484, 1998.

[26] S. M. Shahruz and A. L. Schwartz, "Nonlinear PI compensators that achieve high performance," *J. Dyn. Syst. Meas. Control*, vol. 119, pp. 105–110, 1997.

[27] F. Wang, D. Abramovitch, and G. Franklin, "A method for verifying measurements and models of linear and nonlinear systems," in *Proc. Amer. Control Conf.*, San Francisco, CA, 1993, pp. 93–97.

[28] F. Wang, T. Hurst, D. Abramovitch, and G. Franklin, "Disk drive pivot nonlinearity modeling part II: time domain," in *Proc. Amer. Control Conf.*, Baltimore, MD, 1994, pp. 2604–2607.
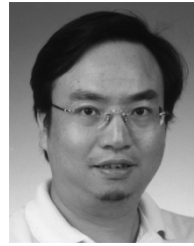
Ben M. Chen (S'89–M'92–SM'00) was born in Fuqing, Fujian, China, in 1963. He received the B.S. degree in computer science and mathematics from Xiamen University, Xiamen, China, in 1983, the M.S. degree in electrical engineering from Gonzaga University, Spokane, WA, in 1988, and the Ph.D. degree in electrical and computer engineering from Washington State University, Pullman, in 1991.

From 1992 to 1993, he was an Assistant Professor in the Electrical Engineering Department, State University of New York at Stony Brook. Since 1993, he has been with the Department of Electrical and Computer Engineering, National University of Singapore, where he is currently a Professor. His current research interests are in robust control, systems theory, and control applications. He is the author/coauthor of seven research monographs including *Linear Systems Theory: A Structural Decomposition Approach* (Boston: Birkhäuser, 2004); *Hard Disk Drive Servo Systems* (New York: Springer-Verlag, 2002); and *Robust and H_∞ Control* (New York: Springer-Verlag, 2000). He was an Associate Editor for *Asian Journal of Control* and *Automatica*, and is currently serving as an Associate Editor of *Control and Intelligent Systems* and *Systems and Control Letters*.

Dr. Chen was an Associate Editor for the IEEE TRANSACTIONS ON AUTOMATIC CONTROL.

Guoyang Cheng (S'03) received the B.Eng. degree in information systems from the Department of System Engineering and Applied Mathematics, National University of Defense Technology, Changsha, China in 1992 and the M.Eng. degree in control engineering from the Department of Automation, Tsinghua University, Beijing, China in 1995. He is currently working toward the Ph.D. degree in the Department of Electrical and Computer Engineering, National University of Singapore.

From 1995 to 2001, he was a Computer Engineer in Xiamen, China. His research interests include robust and nonlinear control, mechatronics, disk drive servo systems, and microelectromechanical systems (MEMS).

Mr. Cheng was a recipient of the Best Industrial Control Application Prize at the 5th Asian Control Conference, Melbourne, Australia (2004).

Kemao Peng was born in Anhui Province, China, in 1964. He received the B.Eng. degree in aircraft control systems, the M.Eng degree in guidance, control, and simulation, and the Ph.D. degree in navigation, guidance and control, all from Beijing University of Aeronautics and Astronautics, Beijing, China, in 1986, 1989, and 1999, respectively.

From 1998 to 2000, he was a Postdoctoral Research Fellow in the School of Automation and Electrical Engineering, Beijing University of Aeronautics and Astronautics. Since 2000, he has been a Research Fellow in the Department of Electrical and Computer Engineering, National University of Singapore. His current research interests are in the applications of control theory to servo systems. He is a coauthor of a monograph, *Hard Disk Driver Servo Systems*, 2nd Edition (New York: Springer-Verlag, 2005, in press).

Dr. Peng was a recipient of the Best Industrial Control Application Prize at the 5th Asian Control Conference, Melbourne, Australia (2004).

Tong H. Lee received the B.A. degree (First Class Honors) in the Engineering Tripos from Cambridge University, Cambridge, U.K., in 1980 and the Ph.D. degree from Yale University, New Haven, CT, in 1987.

He is currently a Professor in the Department of Electrical and Computer Engineering, National University of Singapore. His research interests are in the areas of adaptive systems, knowledge-based control, intelligent mechatronics, and computational intelligence. He is an Associate Editor for *Automatica*, *Control Engineering Practice*, the *International Journal of Systems Science*, and *Mechatronics*. He has also co-authored three research monographs, and holds four patents (two of which are in the technology area of adaptive systems, and the other two are in the area of intelligent mechatronics).

Dr. Lee is currently an Associate Editor for the IEEE TRANSACTIONS ON SYSTEMS, MAN AND CYBERNETICS. He was a recipient of the Cambridge University Charles Baker Prize in Engineering.